CAPELLA INSAR AND PSI TEST: MEXICO CITY

Urs Wegmüller, Christophe Magnard

This document describes the InSAR and PSI test conducted on a Capella data stack over Mexico City, Mexico.

Summary

A stack of 18 Capella scenes acquired with approximately 3-day time intervals and reasonably short spatial baselines (mostly < 500m relative to a centered spatial reference) over a section of Mexico City, was used to assess the possibility of using Differential Interferometry and Persistent Scatterer Interferometry (PSI). Thanks to the short time intervals and reasonably short spatial baselines differential interferograms with high coherence could be generated over this predominantly urban site. PSI with single and multi-reference stacks could be successfully done. The spatial and temporal baselines are not correlated, permitting to estimate both point height corrections and deformation rates. The total time covered by the sequence between 20240626 and 20240815 is only 47.2 days (with an average interval of 2.78 days between two subsequent acquisitions. As a result, the estimation error for the deformation rates is very high. Even after subtracting atmospheric phase the statistical estimation error is of the order of 1cm/year. The statistical point height estimation, on the other hand, is quite accurate (around 0.5m), thanks to the relatively long baselines which are part of the stack.

Capella data stack over Mexico City

X-band HH-pol. SLC stripmap mode data acquired by CAPELLA-C14, operated in a mid-inclination orbit, on 18 dates between 20240626 and 20240815, were used.

Here some characteristics of the data:

- range pixel spacing:	0.62 m
- azimuth pixel spacing:	1.06 m
- heading angle:	44 deg
- incidence angle:	41 deg

The Doppler spectra are strongly overlapping with Doppler Centroid values between -452 Hz and -266 Hz.

Figure 1 shows the time-baseline plots for the single reference stack and a multi-reference stack with baselines < 500m. It shows that the orbital control supports acquiring interferometric pairs with short baselines as well as stacks suited for interferometric time-series analysis.

Differential interferometry

Examples of differential interferograms are shown in Figure 2. To get approximately square pixels we applied a multi-looking with 4 range and 4 azimuth looks. Overall, the X-band differential interferometric phase looks quite “wild”. The main phase components visible are the atmospheric path delay phase, deformation phase, and sometimes an overall phase ramp. With a single interferogram, the different phase terms cannot easily be separated. Based on the three interferograms shown in Figure 2 it is difficult to reliably indicate the overall deformation pattern that is present. For this, a consistent multitemporal analysis is needed (see below). Alternatively, interferograms where one of the components should dominate can be considered. Interferograms with a short temporal interval and a relatively long spatial baseline

are suited to check if residual topographic phase is present. Even better suited is the consideration of double difference interferograms, one 3-day interval differential interferogram is subtracted from a second 3-day interval differential interferogram. The resulting double difference interferogram should include only minimal deformation phase, assuming the deformation velocity is the same in the two intervals. Similarly, pairs with a very short spatial baseline can be used individually or pairs can be combined to create a double-difference interferogram with a very short spatial baseline. This ensures a minimal residual topographic phase.

The data set includes pairs with short to long spatial baselines. Figure 3 shows the interferometric phase and the coherence for three pairs with short (~100m), intermediate (~400m) and long (>1000m) baselines. In the case of the long baseline, the interferometric phase is very noisy.

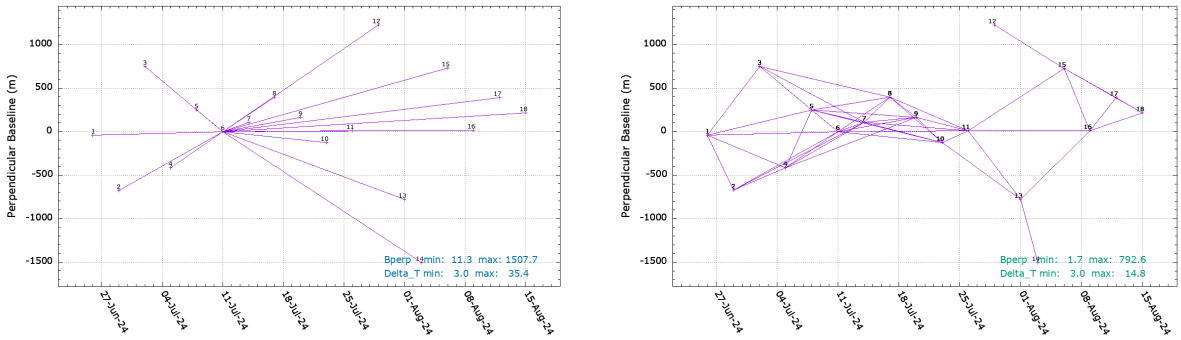

Figure 1 Time-baseline plots for single reference stack (left, reference 20240711) and a multi-reference stack with $\Delta t<15$days and $B_\perp< 800$m.

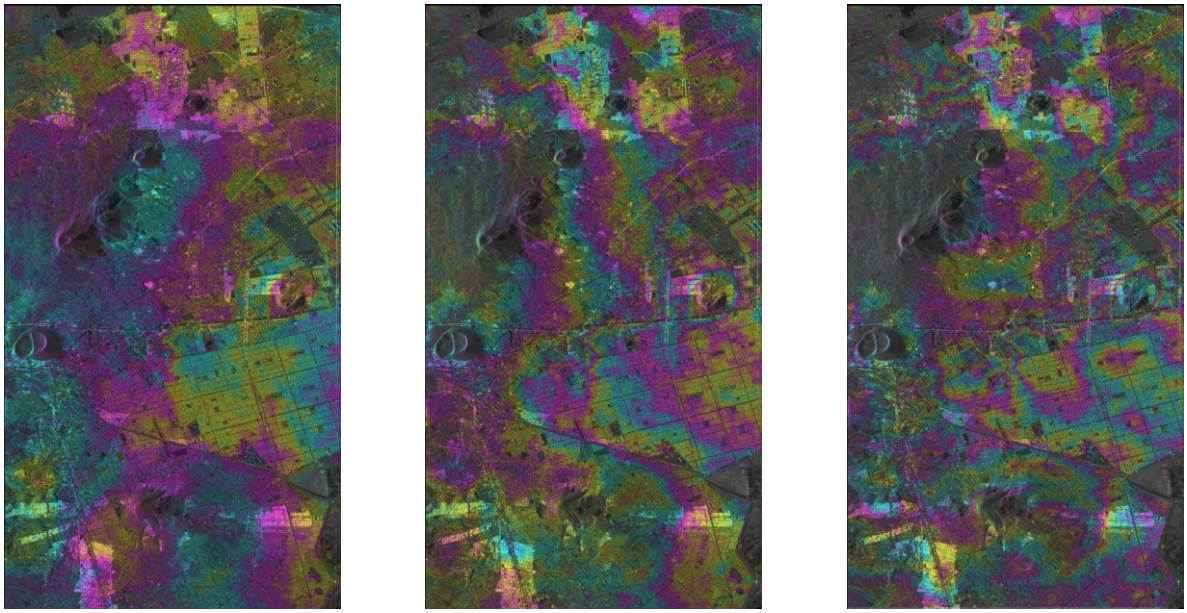

20240626_20240711, dt=14.7d, $B_\perp$= 41m | 20240626_20240726, dt=29.5d, $B_\perp$= 52m | 20240626_20240809, dt=44.2d, $B_\perp$=28m

Figure 2 Examples of differential interferograms with very short spatial baselines and temporal intervals between 14 and 44 days.

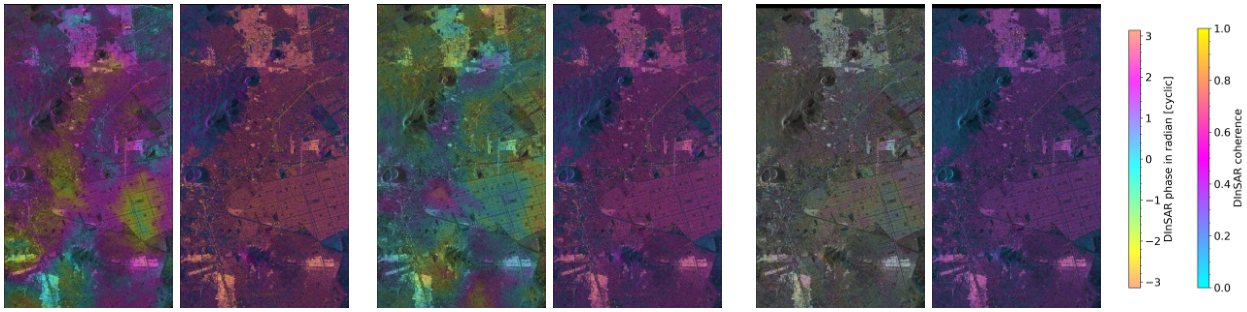

20240711_20240714, dt=2.9d, B⊥=105m | 20240711_20240717, dt=5.9d, B⊥=399m | 20240711_20240729, dt=17.7d, B⊥=1225m

Figure 3 Examples of differential interferogram phase (left) and coherence (right) of pairs with short to long spatial baselines.

Interferometric time-series analysis

Different types of interferometric time-series analyses can be used. Important characteristics include if a single reference stack or a multi-reference stack is considered and if single pixel phases or multi-look interferometric phases are considered. In the following we discuss two different approaches that we tested:

(a) an approach using multi-look interferometric phases with a multi-reference stack,
(b) a typical "Persistent Scatterer Interferometry" approach considering single pixel phases of "point scatterer candidates" with a single reference stack.

a) Multi-reference stack with DInSAR phases

The multi-reference stack used includes all pairs with spatial baselines below 800m and temporal intervals up to 15 days (Figure 1). For each of the selected pairs the differential interferogram was calculated with 4 range and 4 azimuth looks using the Copernicus 3-arc-second DEM as topographic reference for the geocoding and the simulation of the topographic and orbital phase.

The phase unwrapping included a spatial unwrapping step and then an iterative checking and correcting step considering the consistency of the multi-reference stack. The multi-reference stack includes redundant observations, i.e. an interval is covered by several interferograms. In the case of few unwrapping errors the redundance was used to identify and correct unwrapping errors present in individual interferograms.

The temporal and spatial baselines of the multi-reference stack used are not much correlated. Consequently, it was possible to estimate both the deformation time series and a height correction. The atmospheric phase was estimated by calculating the difference between the temporally unfiltered time series and a temporally filtered time series. The phase standard deviation between the phase values of the individual differential interferograms and the modeled phase, which is the sum of the deformation phase and the atmospheric phase, can be used as a quality characteristic to mask estimates with low quality. Higher phase standard deviations relate to high phase noise (i.e. low coherence), unwrapping errors, or unmodelled topographic, deformation or atmospheric phase. A linear regression through the deformation time series was used to calculate the average deformation rate.

The selection of the spatial reference point was difficult (see Figure 4 for the location chosen). Positive displacement rates indicate that the reference location may not be fully stable but may be slightly subsiding – which explains the observed positive LOS displacement rates.

The average deformation rate, using a threshold of 0.8 radian for the phase standard deviation, is shown in Figure 4. Very high line-of-sight (LOS) rates, with maximum values above 70cm/year, corresponding to assumed vertical displacements above 90cm/year, are observed. The deformation time series is shown in Figures 5 and 6.

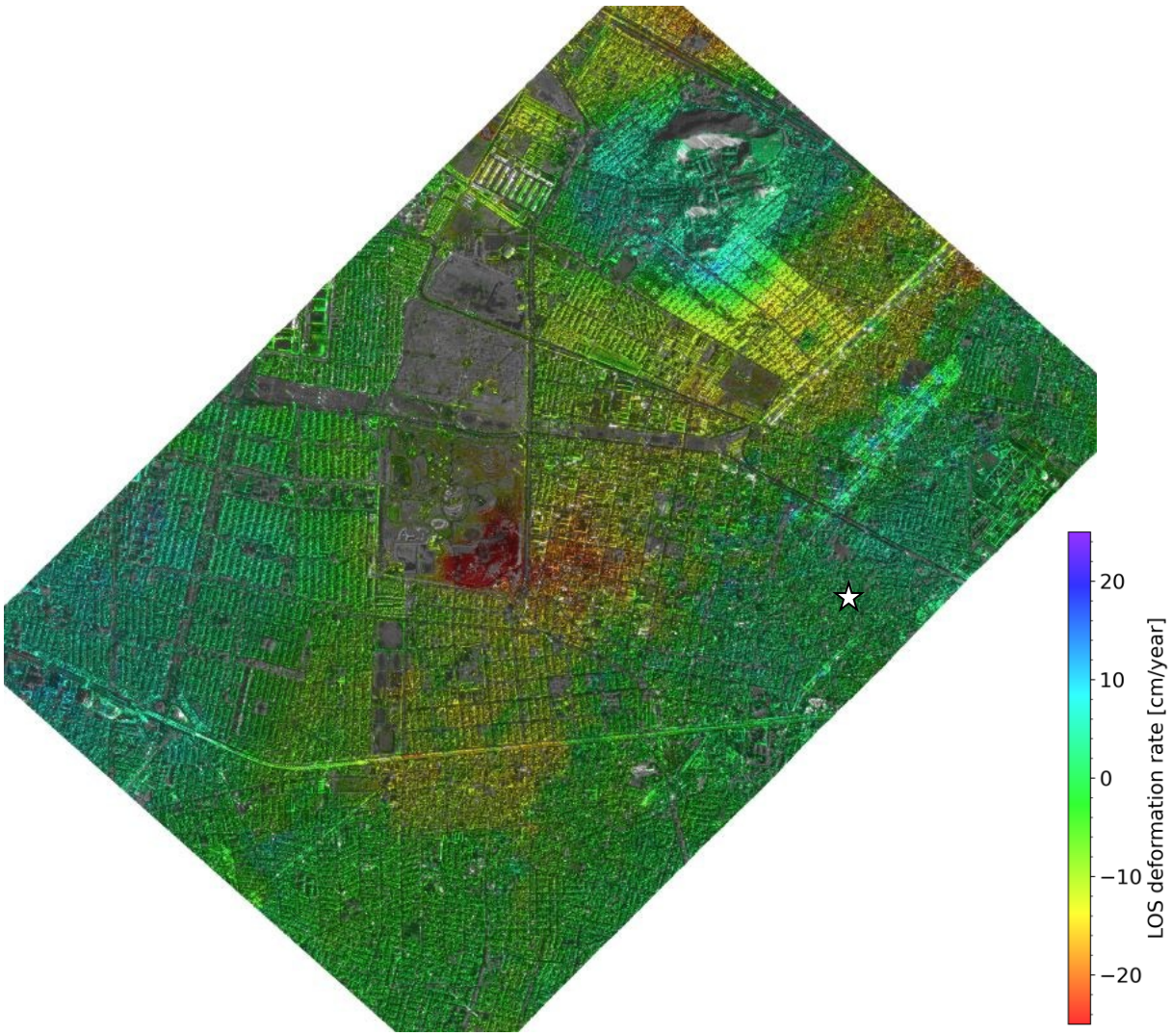

Figure 4 Average line-of-sight deformation rate determined based on 18 Capella acquisitions between 26-Jun-2024 and 15-Aug-2024. The spatial reference point used is indicated with a white star. In gray areas the result has been masked based on a phase standard deviation exceeding 0.8 radian relative to the temporally filtered time series. In the red area near the center of the image maximum LOS rates above 70cm/year are observed (corresponding to assumed vertical displacements above 90cm/year).

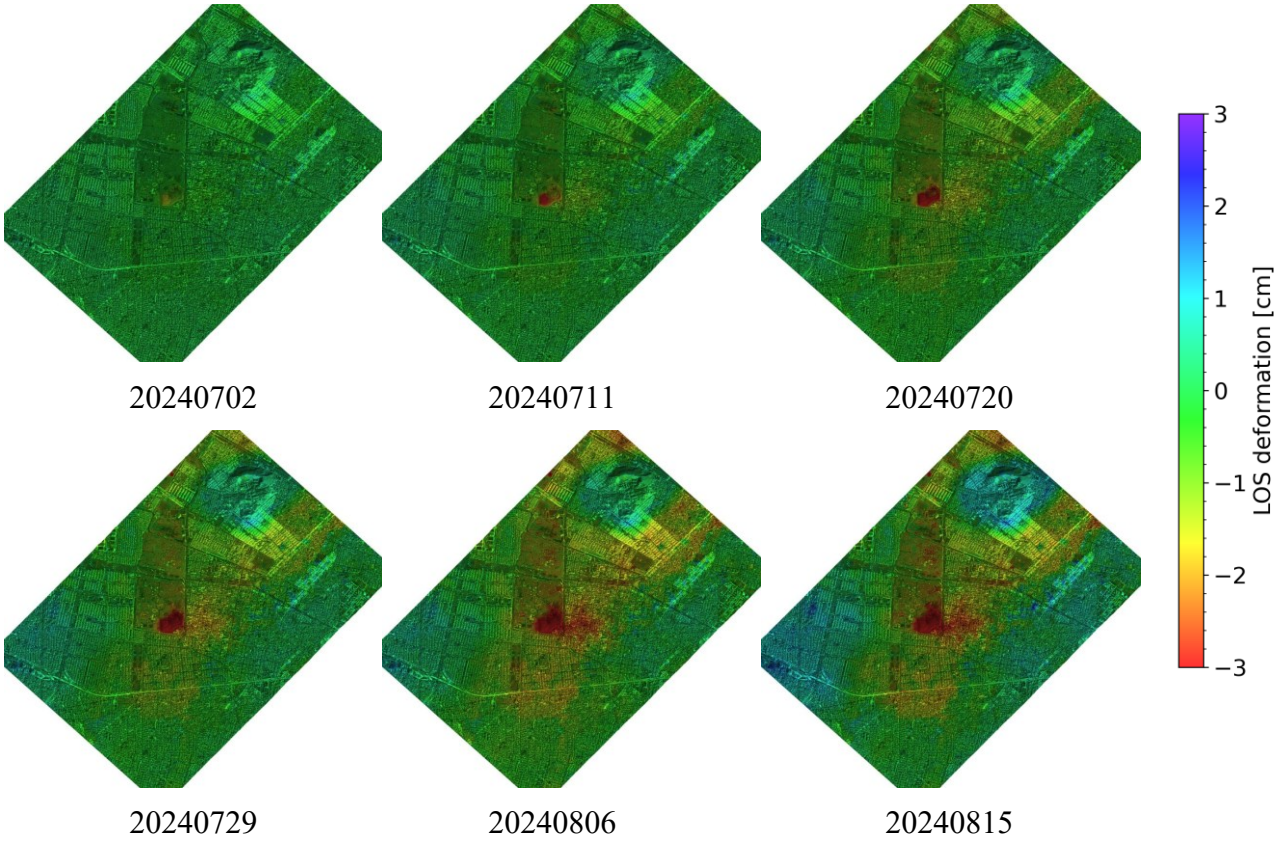

Figure 5 Line-of-sight deformation time series (only every third date is shown) determined based on 18 Capella acquisitions between 26-Jun-2024 and 15-Aug-2024.

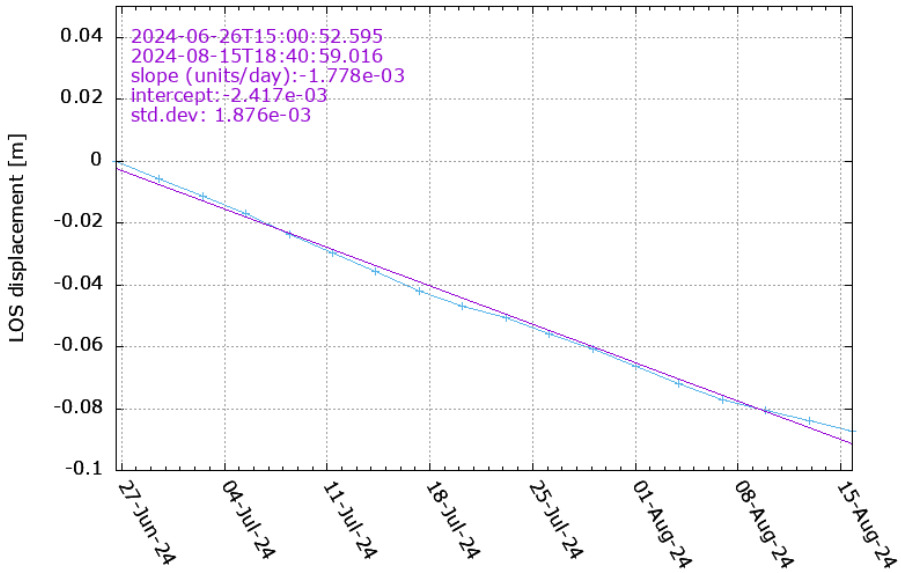

Figure 6 Displacement plot for a fast-moving area in the southern part of the Cuitlahuac Park. The average rate corresponds to -65cm/year in the line-of-sight direction. The rate seems to be quite constant for the observation period.

In Figure 7, we examine the estimated atmospheric phases, also to verify whether non-uniform motion phase has been mistakenly attributed to the atmospheric phase.

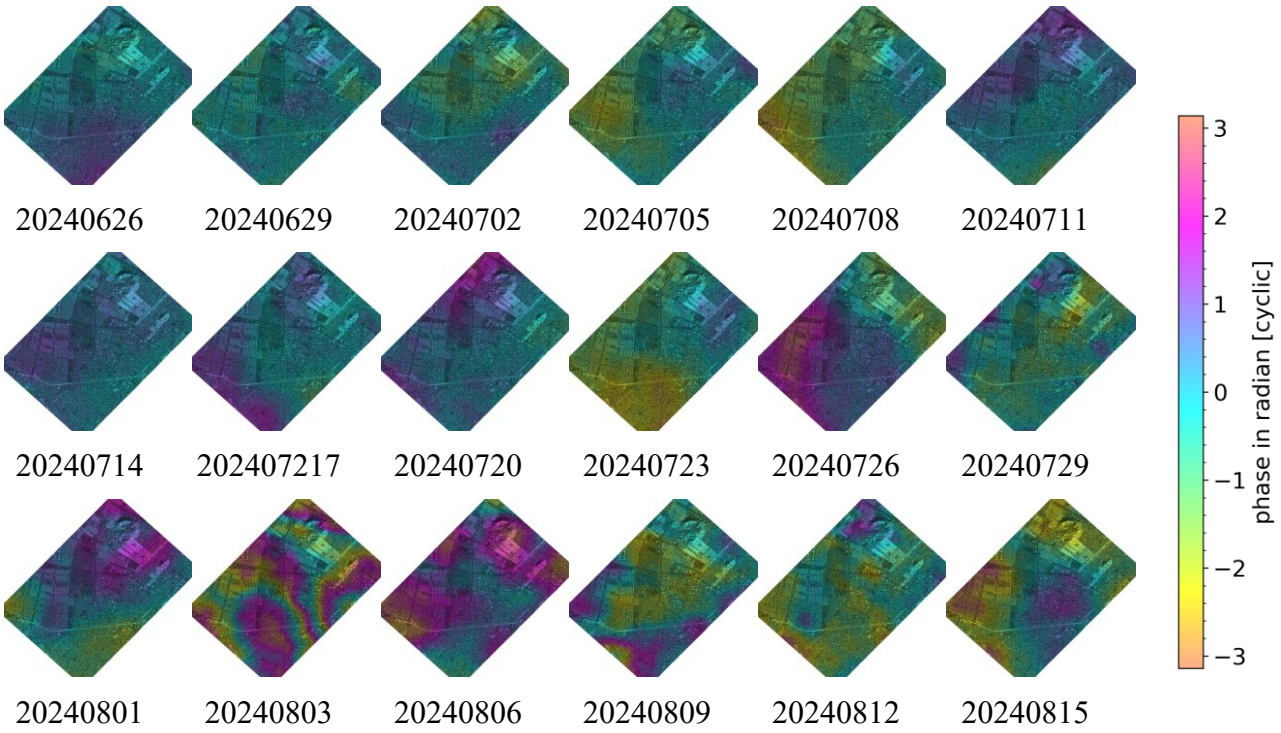

Figure 7 Atmospheric phase estimated for the 18 Capella acquisitions between 26-Jun-2024 and 15-Aug-2024.

b) Persistent Scatterer Interferometry

Persistent Scatterer Interferometry (PSI) is applicable to data sets acquired over long time spans. A major advantage of the persistent scatterers is that they remain coherent over very long periods. Typically, persistent scatterers correspond to “hard targets” such as infrastructure (e.g. buildings) and rocks. PSI can also be applied to a data set acquired over a short time period, but the precision of the estimated average deformation rate is lower.

One strength of PSI is that it is also applicable for stacks including long spatial baselines. To achieve this, single-pixel phase values need to be used. For point like scatterers the phase remains coherent also for long spatial baselines.

We conducted a PSI test using single pixel phases and using a single reference stack. In an initial step, persistent scatterer candidates were determined. The two main criteria considered were (1) the spectral diversity (which is low for point-like scatterers), and (2) the temporal variation of the single pixel scatter intensity (which is low for points with high temporal coherence). About 6.3 million candidates were used. Out of these a result could be determined for about 4.7 million points. This is a high fraction of the candidates (75%), which indicates that more points could be included in the candidate list and solution.

Then, an average deformation rate, a point height correction (relative to the Copernicus DEM height), an atmospheric phase, and the residual phase (phase difference between measured and modeled value) are determined in a two-dimensional regression analysis. This procedure

is iterated a few times. The resulting average deformation rate and height correction are shown in Figures 8 and 9. The related statistical estimation errors (considering the phase deviations after subtracting the estimated atmospheric phase) are of the order of 25cm for the height correction and 1cm/year for the average deformation rate.

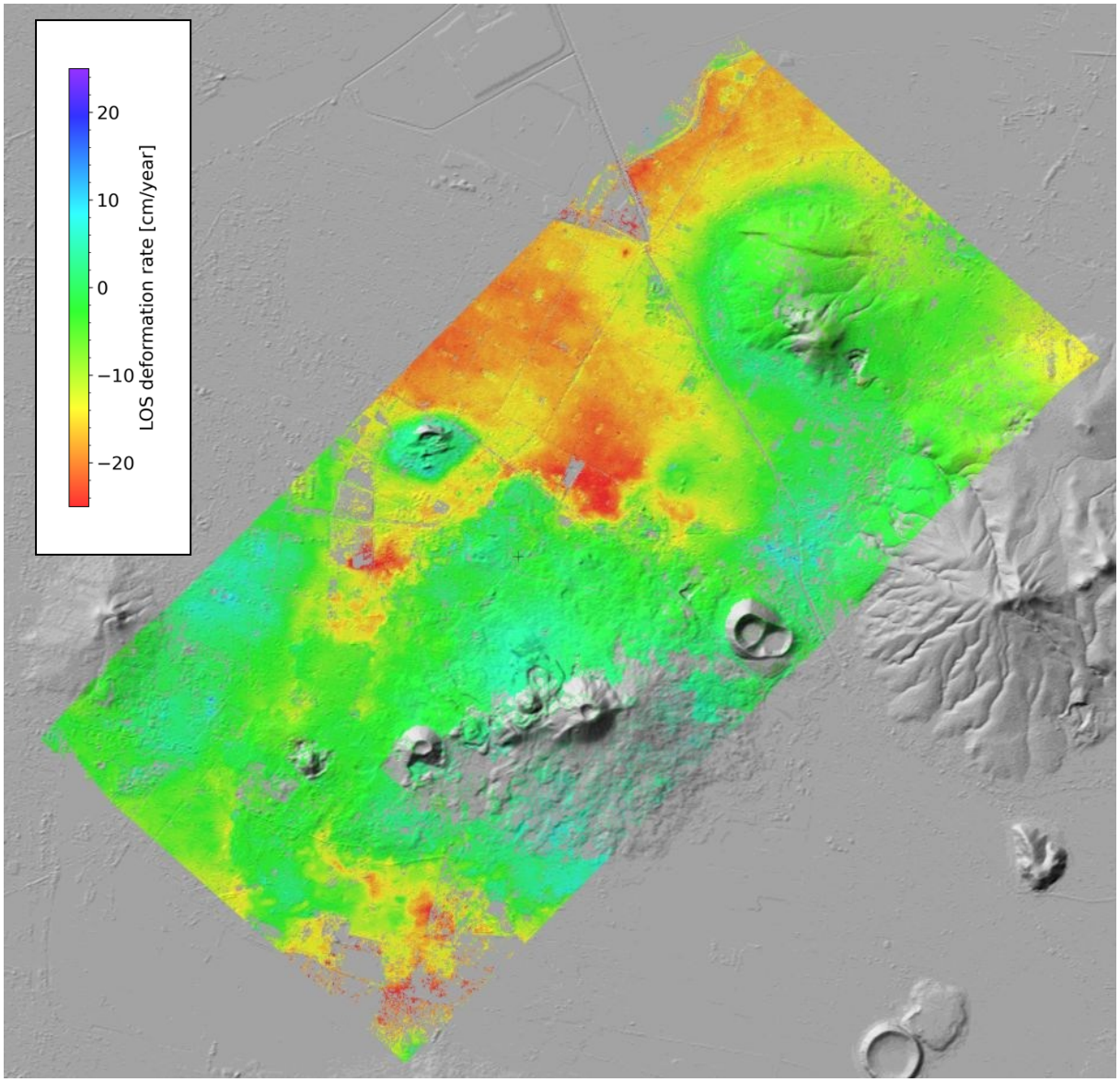

Figure 8 Average line-of-sight displacement rate determined in the single reference stack PSI analysis for the 18 Capella acquisitions between 26-Jun-2024 and 15-Aug-2024.

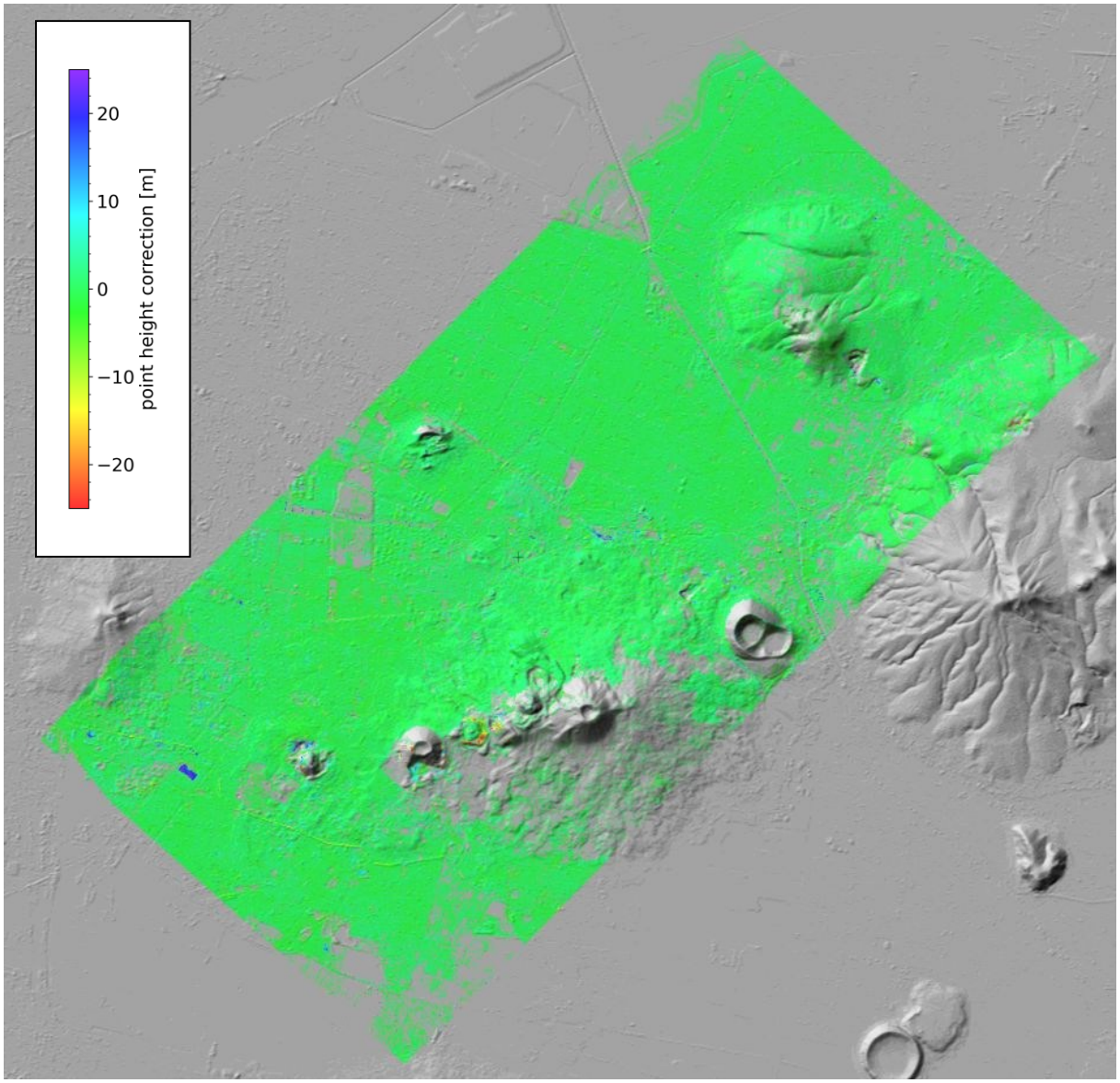

Figure 9 Point height correction determined in the single reference stack PSI analysis for the 18 Capella acquisitions between 26-Jun-2024 and 15-Aug-2024.

A detailed view of the average deformation rate is shown in Figure 10. Notice that the points align nicely along linear structures when considering the corrected point height in the geocoding. The detailed view also shows how much the point density differs spatially. There are many points along the subway line, but hardly any on the road and the vegetated separation between the roads. An example of time series is shown in Figure 11.

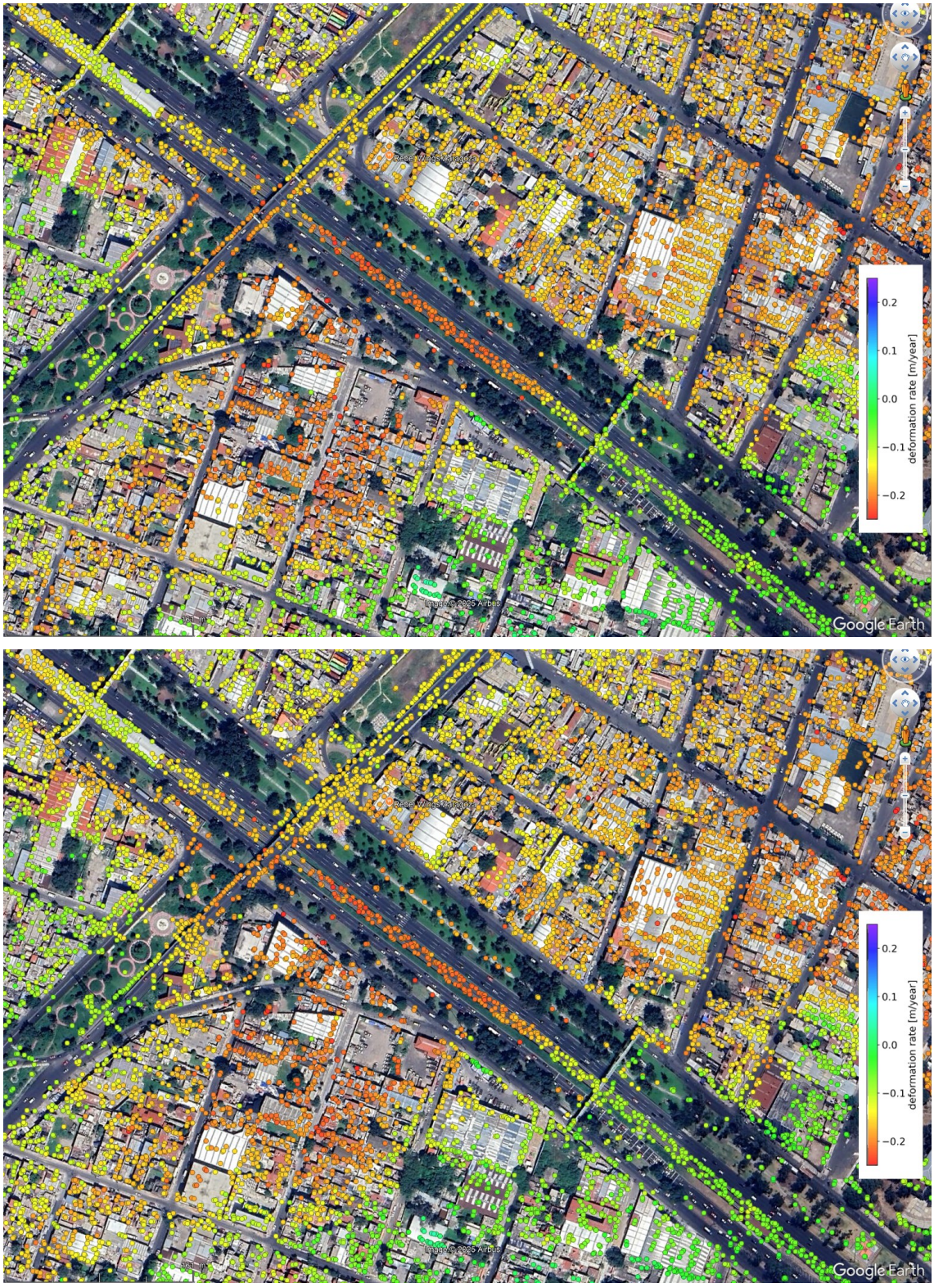

Figure 10 Detailed view of average line-of-sight displacement rate determined in the single reference stack PSI analysis for the 18 Capella acquisitions between 26-Jun-2024 and 15-Aug-2024. The corrected point height was considered in the geocoding of the top image, while the Copernicus DEM height was used in the bottom image.

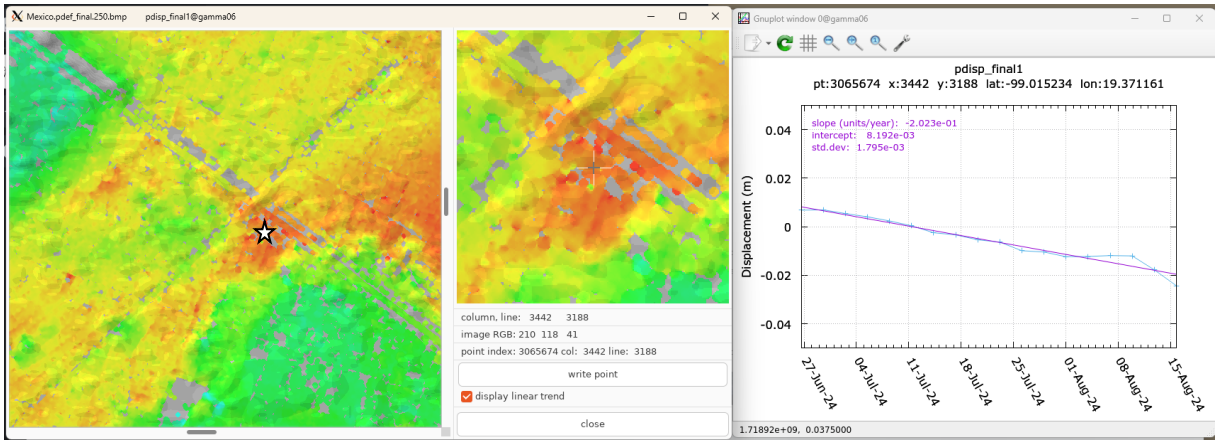

Figure 11 Displacement time series for a location in a subsiding area.

Backscatter and coherence

Averaging a stack of co-registered backscattered images permits generating an average backscatter image with a significantly increased signal to noise level. Furthermore, the coherence can be estimated for each interferometric pair. The backscatter and coherence can provide information on the land cover. Figure 12 shows an RGB composite of the average of the coherence of all 3-day pairs (red channel, linear scale), the average radar backscatter (green channel, log scale), and the temporal variability of the backscatter (blue channel, log scale). Buildings show yellow colors (high coherence, high backscatter), vegetated areas show green colors (low coherence, intermediate backscatter). Water surfaces and other areas with significant temporal change in the backscatter (and low coherence) show blue colors.

Conclusions

The uncommon orbit inclination of CAPELLA-C14 has the potential to enhance displacement measurements in the North-South direction compared to conventional polar orbits. Combining line-of-sight (LOS) displacement results from ascending and descending mid-inclination orbits, possibly in conjunction with results from polar orbits, would further improve the retrieval of 3D displacement vectors.

The X-band HH-pol. SLC stripmap mode data acquired by CAPELLA-C14, operated in a mid-inclination orbit, on 18 dates between 20240626 and 20240815, over Mexico City, were successfully used for DInSAR and PSI.

All the technical steps (e.g. geocoding, co-registration, interferogram generation) worked well.

The PSI result provides for the selected point like scatterers high quality topographic heights and displacement information.

The calculated height estimation error was around 0.25m. The heights could not be validated in detail, but considering the estimated height in Google Earth shows that the location and spatial variation correspond well to the image context.

The estimated deformation rate clearly shows the ongoing fast subsidence, in spite of the short overall total time interval covered by the stack. Because of the short overall time span covered by the data the estimation errors are at 1cm/year level, but this is sufficient in this area with subsidence rates up to more than 20cm/year. Considering an overall longer total time interval would significantly increase the precision of the deformation rate estimation.

Using the backscatter and coherence an RGB composite of the average coherence, average backscatter and backscatter temporal variability was calculated for the Capella X-band stack, which provides information about the land cover.

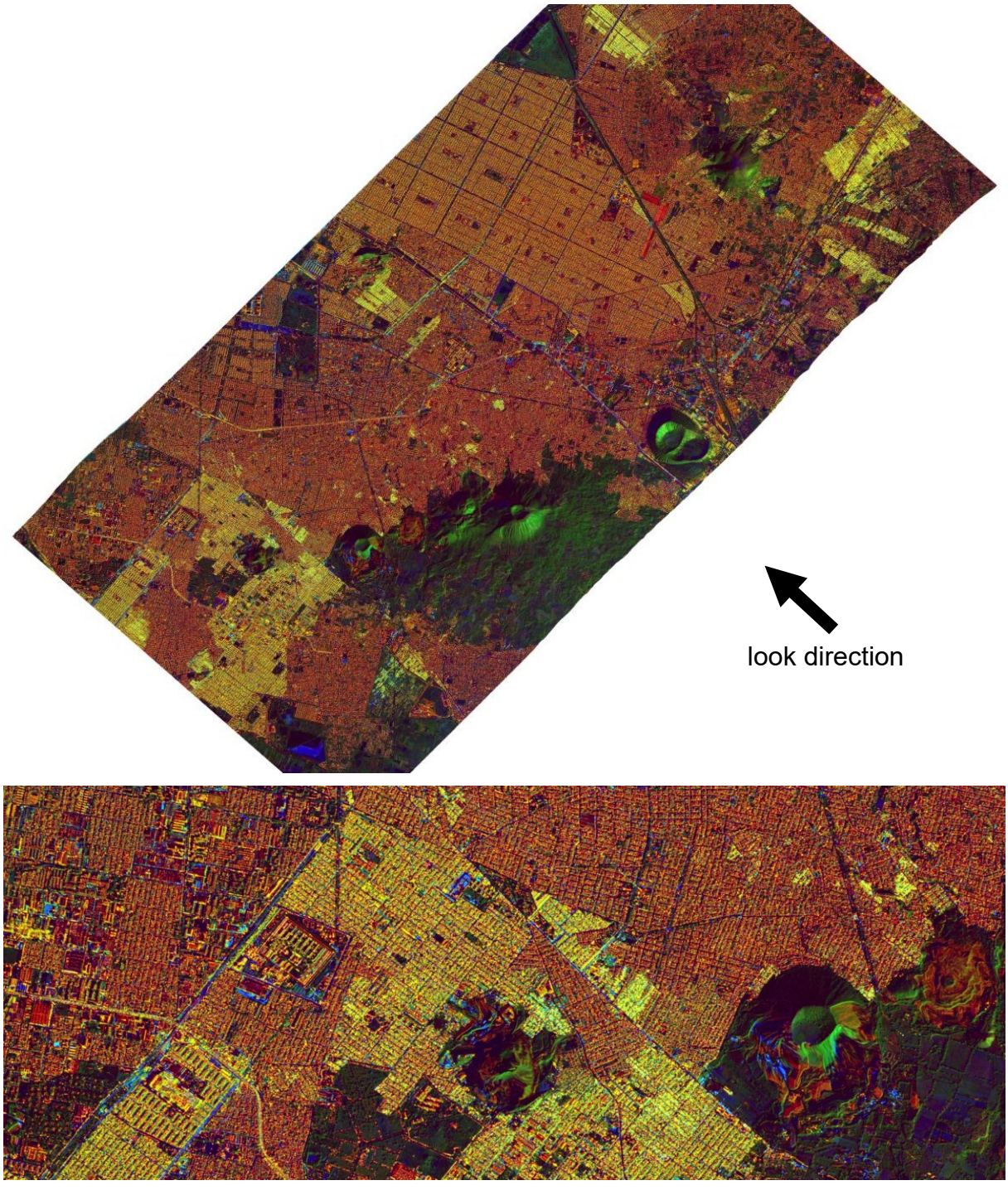

Figure 12 RGB composite of average coherence, average backscatter and backscatter temporal variability calculated for the Capella X-band stack over Mexico City. The top image shows the complete area covered by the stripmap acquisitions; the bottom image is a more detailed view on a smaller section. The arrow indicates the radar look direction (at 40.5 deg. incidence angle). Yellow areas correspond primarily to buildings with very high backscatter from structures oriented perpendicular to the look direction.

Acknowledgement

Capella is acknowledged for providing the SLC data used in this work through the CAPELLA SPACE INSAR PILOT AGREEMENT with GAMMA. The original data is copyright CAPELLA SPACE. The data was processed by GAMMA, using the GAMMA Software.